Journal of Thermal Science Vol.33, No.1 (2024) 328–347

https://doi.org/10.1007/s11630-023-1896-6 **Article ID: 1003-2169(2024)01-0328-20**

Supercritical CO_2 Cycles for Nuclear-Powered Marine Propulsion: Preliminary Conceptual Design and Off-Design Performance Assessment

LI Zhaozhi, SHI Mingzhu, SHAO Yingjuan*, ZHONG Wenqi

Key Laboratory of Energy Thermal Conversion and Control of Ministry of Education, School of Energy and Environment, Southeast University, Nanjing 210096, China

Abstract: Using the efficient, space-saving, and flexible supercritical carbon dioxide (sCO_2) Brayton cycle is a promising approach for improving the performance of nuclear-powered ships. The purpose of this paper is to design and compare sCO_2 cycle power systems suitable for nuclear-powered ships. Considering the characteristics of nuclear-powered ships, this paper uses different indicators to comprehensively evaluate the efficiency, cost, volume, and partial load performance of several nuclear-powered sCO_2 cycles. Four load-following strategies are also designed and compared. The results show that the partial cooling cycle is most suitable for nuclear-powered ships because it offers both high thermal efficiency and low volume and cost, and can maintain relatively high thermal efficiency at partial loads. Additionally, the new load-following strategy that adjusts the turbine speed can keep the compressor away from the surge line, making the cycle more flexible and efficient compared to traditional inventory and turbine bypass strategies.

Keywords: supercritical CO_2 cycle; nuclear; marine propulsion; off-design performance

1. Introduction

The emergence of climate change as a major challenge of the century has inspired significant progress in sustainable behaviours and technologies. In 2018, greenhouse gas emissions from fossil-fueled ships accounted for 2.89% of global greenhouse gas emissions, and the International Maritime Organization has projected that these emissions will increase by 50% by 2050 [1]. Among the various types of engines, nuclear-powered engines have the greatest potential for reducing CO_2 emissions. They also offer advantages such as high single-engine power and long endurance, which are not present in commonly used gas turbine engines, fossil-fuel steam engines, and diesel engines. As constraints on the use of fossil fuels in transportation become more stringent, the use of marine nuclear propulsion may become more widespread.

The steam Rankine cycle has been widely used in power conversion systems for nuclear power plants, naval ships, submarines, and icebreakers due to its mature technology and relatively acceptable efficiency and system reliability at reactor operating temperatures below 350°C [2]. However, achieving high thermal efficiency with the steam Rankine cycle often requires complex construction, such as the use of over 30 turbine stages in some cases [3]. In the case of ships, where space is limited, improving the power density of the power system can increase cargo capacity. As an alternative, the sCO_2 cycle offers compact turbomachinery, a simple cycle layout, and excellent cycle efficiency at medium turbine inlet temperatures (450°C–600°C) [4–15].

Received: Sep 8, 2022 AE: XIE Jian Corresponding author: SHAO Yingjuan E-mail: yjshao@seu.edu.cn

Nomenclature

Abbreviations

AT	Auxiliary turbine
EP	Electric propulsion
HTR	High temperature recuperator
IHX	Intermediate heat exchanger
LFR	Lead-cooled fast reactor
LTR	Low temperature recuperator
MCOM	Main compressor
MP	Mechanical propulsion
MT	Main turbine
PC	Partial cooling cycle
PCHE	Printed circuit board heat exchanger
PCOM	Pre-compressor
PWR	Pressurized water reactor
RC	Recompression cycle
RCOM	Recycled compressor
sCO_2	supercritical CO_2
SFR	Sodium-cooled fast reactor
SR	Simple recuperative cycle
Tur	Turbine

Symbols

C	Cost/USD
C_{BM}	The price of PCHE in per unit mass/USD·kg^{-1}
CEP	The cost of every unit of cycle output power/USD·kW^{-1}
D	Diameter/m
d_c	Diameter of micro-channel/mm
E_{input}	Exergy input to the sCO_2 cycle/MW
e	Specific exergy/kJ·kg^{-1}
f_c	Moody friction coefficient
f_m	The fraction of metal
H	Height of PCHE/m
h	Specific enthalpy/kJ·kg^{-1}
Δh	Isentropic enthalpy change/kJ·kg^{-1}
htc	Heat transfer coefficient/ kW·(m^2·K)$^{-1}$
HC	Heat capacity/W·K^{-1}
I_x	Irreversibility of the xth component/%
L	Length of heat exchanger/m
m	Mass flow rate/kg·s^{-1}
m_t	Total turbine mass flow rate/kg·s^{-1}
N	Shaft rotational speed/r·min^{-1}
N_1	The number of sub-exchangers
N_2	The number of modules
NTU	The number of transfer units
Nu	Nusselt number
n_s	Isentropic volume exponent
P_{ti}	Turbine inlet pressure/MPa
P_{to}	Turbine outlet pressure/MPa
ΔP	Pressure drop of heat exchanger/kPa
p_c	Channel pitch/mm
Pe	Peclet number
Pr	Prandtl number
Q	Total heat load of the heat exchanger/MW
Q_{th}	Thermal duty of the reactor/MW
q	The heat load of the sub-heat exchanger/MW
R	Gas constant/J·(kg·K)$^{-1}$
Re	Reynolds number
T_{min}	Cycle minimum temperature/°C
T_{ti}	Turbine inelt temperature/°C
ΔT_{IHX}	Pinch temperature difference of IHX/°C
ΔT_r	Pinch temperature difference of recuperator /°C
t	The thickness of the plate/mm
UA	Thermal conductance of heat exchanger/ W·K^{-1}
V_{HX}	Total volume of the cycle heat exchangers/m^3
v	Specific volume/m^3·kg^{-1}
W	Width of PCHE/m
W_a	Total electricity consumption of auxiliary facility and daily demand/MW
W_{AT}	Power of the auxiliary turbine/MW
W_C	Power of compressor/MW
W_{MT}	Power of the main turbine/MW
W_{net}	Net power output of sCO_2 cycle/MW
W_p	Propulsion power/MW
W_t	Power of turbine/MW
Z	Gas compressibility

Greek letters

ε	Effectiveness of heat exchanger
η_c	Compressor isentropic efficiency/%
η_{ex}	Exergy efficiency of the sCO_2 cycle/%
η_g	Generator efficiency/%
η_{gb}	Gearbox efficiency/%
η_m	Motor efficiency/%

(Continued Table)

η_t	Turbine isentropic efficiency/%	**Subscripts**	
η_{th}	Thermal efficiency of sCO_2 cycle/%	avg	Average value
η^*	Dimensionless efficiency	cold	Heat exchanger cold side
ρ_m	The density of the PCHE material/kg·m^{-3}	d	Design condition
λ	The thermal conductivity of the heat exchanger material/W·(m·K)$^{-1}$	eq	Equivalent value at turbomachine map conditions
φ^*	Dimensionless flow	hot	Heat exchanger hot side
Ψ^*	Dimensionless head	od	Off-design condition

The expansion ratio of the sCO_2 cycle is usually 2–4, and the density of CO_2 is still larger than that of steam at high temperatures [16, 17]. Therefore, it is worthwhile to explore the use of the sCO_2 cycle instead of the steam cycle for energy conversion on nuclear ships. Combs [18] conducted a thermodynamic analysis and preliminary design for the sCO_2 cycle used for conventionally powered naval vessels and concluded that its utilization can increase efficiency and reduce fuel consumption compared to the gas turbine. Oh et al. [3] designed the trans-critical CO_2 cycle for nuclear-powered icebreaking merchant ships travelling on the Northern Sea Route and demonstrated its controllability with a pressurized water reactor (PWR) under icebreaking conditions and its safety through transient analysis [19]. These studies confirm the feasibility of using the sCO_2 cycle as a heat-to-power conversion system on nuclear-powered ships or conventionally-powered ships.

Due to the secrecy surrounding its technology, there is limited published literature on the application of sCO_2 power cycle systems to nuclear-powered ships. However, available information suggests that over the past two decades, the application of the sCO_2 cycle in nuclear power plants has been extensively studied. Moisseytsev and Sienicki [15] compared the cycle efficiencies of four sCO_2 cycles (the recompression cycle, reheating cycle, intercooling cycle and double recompression cycle) when coupled with a sodium-cooled fast reactor (SFR). Li et al. [10] demonstrated that the miniaturized lead-cooled fast reactor (LFR) incorporating a reheating recompression sCO_2 cycle has a higher thermal efficiency and economic advantage over a reactor with a steam-Rankine cycle or a helium Brayton cycle. Pérez-Pichel et al. [20] explored the potential of a basic and improved recompression cycle for use in SFRs and concluded that the basic recompression cycle could achieve a higher efficiency (43.31%) than the steam Rankine cycle. When combined with a bottoming organic Rankine cycle (ORC), the cycle efficiency can be further improved by 0.18%. Zhu et al. [21] compared the performance of a combined sCO_2 cycle when employing an organic Rankine cycle or Kalina cycle as the bottom cycle to recover the exhaust heat of sCO_2 in the cooler, particularly the large amount of afterheat recovery of sCO_2 near the critical point. The results show that the system is more efficient when using R32 or ammonia as the ORC working fluid, with an efficiency enhancement of about 2%. Pham et al. [22] investigated the sCO_2 cycle performance when coupled to a PWR with a turbine inlet temperature (T_{ti}) of 275°C and an SFR with a T_{ti} of 515°C. For the PWR case, the reheating recompression cycle achieved a higher cycle efficiency of 29.3%, while the best cycle efficiency of 43.9% was gained by the intercooling recompression cycle for the SFR. Guo et al. [8] stated that the turbine inlet pressure of 20 MPa is too high to promote the sCO_2 application on SFR, and proposed that adding a dual expansion process to the recompression cycle could reduce the pressure difference in the intermediate heat exchanger (IHX). Yoon et al. [2] evaluated the cycle efficiency and components volume of the sCO_2 cycle when coupled with water-cooled small and medium-sized reactors. Li et al. [11] compared the thermal and economic performance of a miniaturized LFR composed of five different sCO_2 cycles, including the recuperation cycle, pre-compression cycle, partial cooling cycle, recompression cycle, and intercooling cycle.

In the actual sailing scenarios, ships are not always maintained at full speed and full engine load, and the speed and engine load need to be adjusted according to demand. The fast load variation and part-load operation of the engine is an off-design operation scenario that frequently occurs in ship sailing [3]. Research on the off-design performance of the nuclear-powered sCO_2 cycle has primarily focused on its application in nuclear power plants. Floyd et al. [7] investigated the off-design behaviour of the recompression cycle coupled to an SFR as the heat sink temperature varies. Moisseytsev and Sienicki [23] investigated and optimized the load following operation strategy for the air cooling sCO_2 cycle with an AFR-100 reactor. In their work, the turbine bypass approach was used for accurate load control, while inventory control was employed to generally adjust the cycle load to the appropriate amount. Inventory control achieves the purpose of turbine flow and load

regulation by adjusting the CO_2 inventory in the cycle system, i.e. controlling the injection of CO_2 into the cycle from the storage tank or the removal of CO_2 from the cycle to the storage tank, and thereby the pressure at the inlet and outlet of the turbine and compressor is changed due to the variation of mass inventory in the cycle. Oh et al. [24] simulated the part-load operation and accidents of the sCO_2 cycle coupled to a micro modular reactor to verify its safety. Baek et al. [25] analyzed the transient responses of a sCO_2 cycle coupled to PWR under severe load changes showing that the load can decrease from 100% to 10% in 1 second and recover to 90% in 8 seconds. This demonstrates the sCO_2 cycle's ability to quickly and consistently respond to extreme load changes. Carstens [26] investigated different control strategies and part-load operation performance of a single shaft recompression cycle with a turbine inlet temperature of 650°C.

Although most of the current design and analysis of the nuclear-powered sCO_2 cycle is used for nuclear power plants, some of the results can provide reference and guidance for the research of the sCO_2 cycle applied to nuclear-powered ships. When applying the sCO_2 cycle used in nuclear power plants to nuclear-powered ships, the following issues need to be considered. First, the open literature on nuclear-powered sCO_2 cycle mainly paid attention to the recompression cycle or improved recompression cycle which yields higher efficiency. For nuclear-powered ships, where space is limited, the volume, weight and cost of the cycle are also very important, and the cycle efficiency is only one of the indicators that need to be investigated. The investigation and comparison of different sCO_2 cycle layouts coupled with different marine nuclear reactors from various perspectives are required. Second, unlike nuclear power plants, which are generally at full load, ships often maintain a low-speed cruising state. sCO_2 cycles for nuclear-powered ships should be designed to maintain high efficiency and at the part-load. The quantitative analysis and comprehensive comparison of the part-load performance of different nuclear-powered sCO_2 cycles with different load-following control strategies have not been included in the earlier research. Third, due to the need for synchronous power generation in nuclear power plants, the turbine speed remains unchanged when the load changes, but the turbine speed can change with the load change for ship propulsion. In the previous off-design conditions performance study [7, 23, 26–31], the turbine speed was constant. It is necessary to explore the load-following control strategy of the nuclear-powered sCO_2 cycle when the turbine speed changes. Such research could provide valuable insights into the potential of sCO_2 cycles as a power generation technology for nuclear-powered ships.

To explore the potential of using sCO_2 cycles in nuclear-powered ships' propulsion systems and solve the above-mentioned issues, the present work focused on the design, optimization, comprehensive evaluation and comparison of nuclear-powered propulsion systems using different sCO_2 cycles combined with different reactors. Simple recuperation (SR), recompression (RC), and partial cooling (PC) cycles were coupled with mature PWR and advanced Gen-IV SFR reactors, and four load-following control strategies are designed for the nuclear-powered sCO_2 cycle propulsion system. The part-load performance of different systems under different control strategies was compared, and based on the results, the reasonable configuration of the system was discussed. The innovations of this paper are as follows: First, a multi-dimensional evaluation model of the system, considering the thermodynamic and economic performance, heat exchanger and compressor design etc., was established. The different system schemes were compared and analyzed from many aspects to determine the optimal parameters and system design schemes. Second, we proposed new load-following control strategies and compared the thermodynamic performance of nuclear-powered sCO_2 marine propulsion systems under different load-following strategies.

2. System Description

The nuclear-powered sCO_2 cycle marine propulsion system is mainly composed of three parts: the nuclear reactor, the sCO_2 cycle and the propulsion system. This section describes the different system configurations shown in Fig. 1. The split-shaft configuration is applied to ensure the turbine and compressor speed can be adjusted flexibly. The compressor is driven by a separate electric motor, and the speed of the compressor can be flexibly adjusted.

2.1 Marine nuclear reactors

Compared to land-based nuclear reactors, the limited space and load capacity of vessels require marine nuclear reactors to be small and light. Pressurized water reactors, liquid-metal-cooled reactors, and gas-cooled reactors were studied for use in nuclear-powered marine propulsion systems in the 1940s. Because of the low power density and enormous size of gas-cooled reactors, the previous two types of reactors have been used in nuclear-powered ships [32]. Although liquid metal-cooled reactors have higher power density, ship reactors are gradually being monopolized by mature, safe and reliable PWRs due to early material and technology limitations and safety issues. With the in-depth research and development of Gen-IV nuclear reactors in recent years, liquid metal-cooled reactors have made great progress in safety and operability [33]. Combined with

the compact and efficient sCO_2 cycle system, it is believed that the liquid metal-cooled reactors will be strong contenders for application in limited space [11, 15, 34]. Therefore, both PWRs and SFRs are selected to combine with the sCO_2 cycle for nuclear-powered ships in this work. The thermal power of marine reactors can be as low as 10 MW (thermal) (in a prototype) or as high as 200 MW (thermal) in larger submarines and 300 MW (thermal) in surface vessels like the Kirov-class battlecruisers [35]. In addition, two A4W units in Nimitz-class carriers have 550 MW (thermal) each, and the Gerald Ford-class carriers have more potent and straightforward A1B reactors, which are said to have at least a 25% increase in power over A4W, making them 700 MW (thermal) [36]. To facilitate comparative analysis, the thermal power of each reactor is unified to 300 MW (thermal), which is suitable for commercial ships like container vessels [3]. The primary loop parameter of PWRs and SFRs refer to the design of SMART [9], a PWR designed by Korea, and AFR100 [37], an SFR designed by the United States, as described in Table 1.

2.2 sCO_2 cycle

The sCO_2 cycle is coupled with the nuclear reactor coolant system through IHX. Three sCO_2 cycles,

Table 1 Major design parameters of SMART and AFR100 reactor primary loop

Parameter	SMART [9]	AFR100 [37]
Operating pressure/MPa	15	0.1
Core inlet temperature/°C	295.7	373
Core outlet temperature/°C	323	528

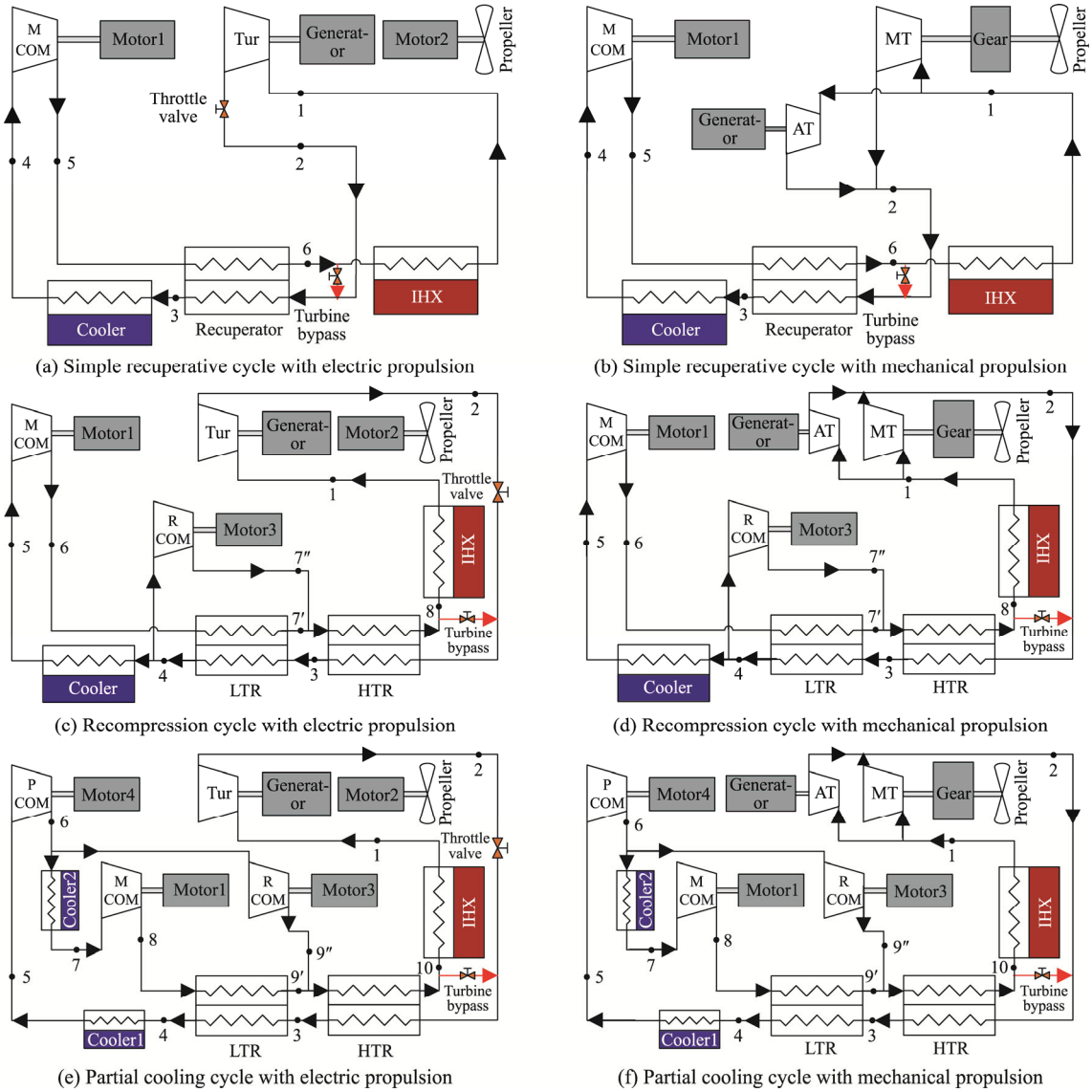

(a) Simple recuperative cycle with electric propulsion

(b) Simple recuperative cycle with mechanical propulsion

(c) Recompression cycle with electric propulsion

(d) Recompression cycle with mechanical propulsion

(e) Partial cooling cycle with electric propulsion

(f) Partial cooling cycle with mechanical propulsion

Fig. 1 Schematic diagram of different nuclear-powered sCO_2 cycle marine propulsion systems

including the SR, RC, and PC, are selected for this study because of their simplicity and/or high thermal efficiency. Their temperature-entropy diagrams are shown in Fig. 2. Earlier authors added intercooling and reheating processes to improve sCO_2 cycle efficiency, but these processes are not considered in this work for the space-limited ships because they increase the system complexity and volume without offering significant efficiency improvement or economic attractiveness [12, 13].

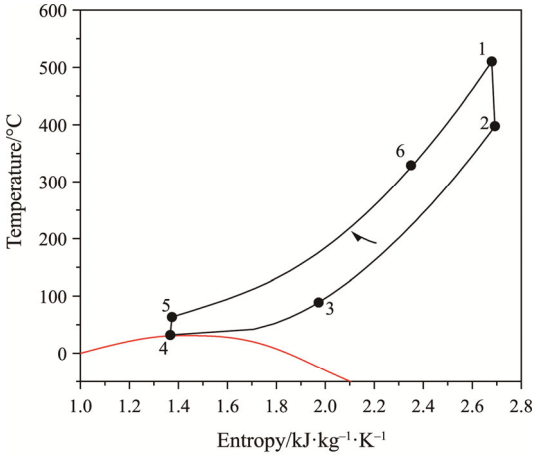

(a) *T-s* diagram of SR using SFR

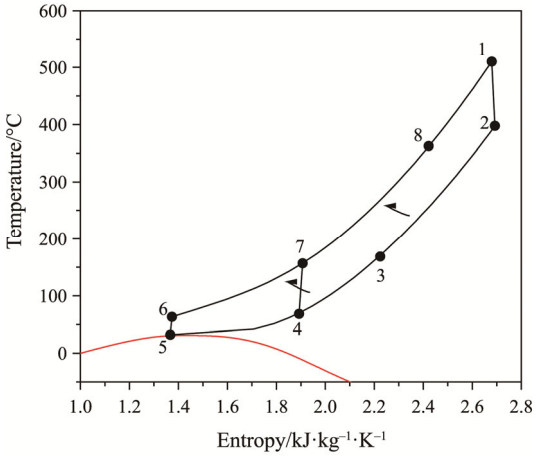

(b) *T-s* diagram of RC using SFR

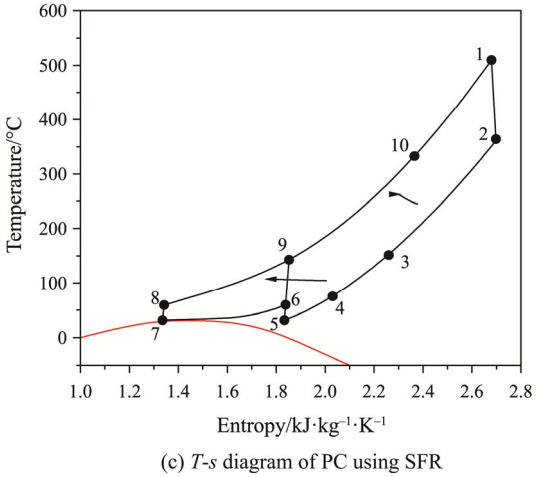

(c) *T-s* diagram of PC using SFR

Fig. 2 *T-s* diagrams of sCO_2 cycles

2.3 Propulsion mode

There are mainly two propulsion modes for ships, mechanical propulsion and electric propulsion [38]. With mechanical propulsion (MP), the main turbine (MT) turns the ship's propeller through a gearbox, and the auxiliary turbine (AT) turns the generator to produce power for auxiliary devices and daily demand. If the electric propulsion (EP) mode is adopted, the turbine first turns the generator and then the ship's propeller is turned by an electric motor. Therefore, the system using the electric propulsion mode is similar to a nuclear power plant, in which the turbine speed is constant as the load changes, while the turbine speed changes as the load changes if the mechanical propulsion mode is adopted. Both mechanical propulsion and electric propulsion method are considered in this paper.

3. Modeling

The main input parameters of the systems shown in Fig. 1 are summarized in Table 2. The net power output (W_{net}) and thermal efficiency (η_{th}) of the sCO_2 cycle are obtained by

$$W_{net} = \sum W_t - \sum W_C \tag{1}$$

$$\eta_{th} = W_{net}/Q_{th} \tag{2}$$

where W_t is the output work of the turbine; W_C is the input work of the compressor and Q_{th} is the thermal duty of the reactor.

The exergy efficiency or the second law efficiency of the cycle (η_{ex}) is given by

$$\eta_{ex} = \frac{\sum W_t - \sum W_C}{E_{input}} = 1 - \sum I_x \tag{3}$$

where E_{input} is the total exergy input to the cycle, and I_x is the irreversibility of the xth component (the ratio of exergy loss in component x to E_{input}).

For the electric propulsion system, the net power delivered to the propeller (W_p) is generated by

$$W_p = \left(W_t \eta_g - \frac{\sum W_C}{\eta_m} - W_a \right) \eta_m \tag{4}$$

where W_a is the total electricity consumption of the auxiliary facility and daily demand and is assumed to be 25 MW [3]; η_g is the gearbox efficiency and η_m is the motor efficiency.

While the propeller shaft power of the mechanical propulsion system is given by

$$W_p = W_{MT} \eta_{gb} \tag{5}$$

in which W_{MT} is the work output of the main turbine and η_{gb} is the gearbox efficiency. The power generated by the

auxiliary turbine (W_{AT}) is

$$W_{AT} = \frac{\sum W_C / \eta_m + W_a}{\eta_g} \tag{6}$$

The economic index CEP (The cost of every unit of cycle output power) is defined as

$$CEP = \frac{C_{PCHE} + C_{com} + C_t}{\sum W_t - \sum W_C} \tag{7}$$

in which C_{PCHE}, C_{com} and C_T are the cost of heat exchangers, compressors and turbines in the sCO_2 cycle, respectively.

Appendix A provides detailed component models and calculation procedures. The calculation results of the recompression cycle are compared with results from Xu et al. [39] to ensure that the component model and cycle calculation process are correct. The settings of the main parameters are consistent with those in their paper, which are as follows: the main compressor inlet pressure is 7.9 MPa; the main compressor outlet pressure varies from 15 MPa to 30 MPa; the turbine inlet temperature changes from 550°C to 850°C; the pressure drop in heat exchanger is 0.13 MPa; the terminal difference of LTR and HTR is 10°C; the turbine isentropic efficiency is 90% and the compressor isentropic efficiency is 89%. As shown in Fig. 3, the largest error between the calculation results of this model and the literature data is less than 1%, showing that the sCO_2 cycle calculation method in this paper is valid.

Table 2 The designed parameters of nuclear-powered sCO_2 cycle marine propulsion system

Parameters	Value
Turbine inelt temperature (T_{ti})	480°C–520°C (SFR) 275°C–315°C (PWR)
Cycle minimum temperature (T_{min})	32°C–40°C
Turbine inlet pressure (P_{ti})	14–28 MPa
Pinch temperature difference of recuperator (ΔT_r)	5°C–15°C
Pinch temperature difference of IHX (ΔT_{IHX})	5°C
Turbine isentropic efficiency (η_t)	93% [13]
Compressor isentropic efficiency (η_c)	89% [13]
Motor efficiency (η_m)	95% [40]
Generator efficiency (η_g)	99% [41]
Gearbox efficiency (η_{gb})	99% [42]

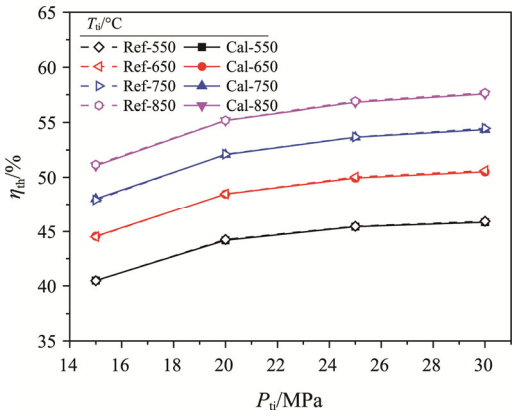

Fig. 3 Comparison of calculation results of recompression cycle efficiency between the present study and those of Xu et al. [39]

4. Results and Discussion

4.1 Design performance

4.1.1 Design performance of sCO_2 cycle with SFR

Thermal efficiency (η_{th}), exergy efficiency (η_{ex}) and net output power (W_{net}) are important indicators of the sCO_2 cycle's thermal performance, while CEP can reflect the economic performance of the system. The heat exchanger volume (V_{HX}) can be used as a reference for the sCO_2 cycle system's volume in space-constrained ships, as it is the largest volume component of the cycle. The mass flow rate of sCO_2 (m_{sCO_2}) is related to the auxiliary system's weight and volume, and affects the selection of the pipeline's diameter and wall thickness, as well as the size of the storage tank. This section explores the system's design performance under different design parameters, including cycle minimum temperature, recuperator pinch temperature, turbine inlet temperature, and turbine inlet pressure, which have significant impacts on the system's performance.

Fig. 4 shows the performance of the three sCO_2 cycles when coupled with SFR under different cycle minimum temperatures (T_{min}) and recuperator pinch temperatures (ΔT_r). Fig. 5 depicts the performance of the three SFR-coupled cycles at various turbine inlet temperatures (T_{ti}) and turbine inlet pressures (P_{ti}). Some data are missing from the RC performance graph because the

Table 3 Effects of design parameter changes on sCO_2 cycle performance when coupled with SFR ('+' means positive effect; '–' means negative effect)

Variables	η_{th}	η_{ex}	m_{sCO2}	CEP	V_{HX}	W_{net}
T_{min}	–	–	+	+	+(RC) +(SR) –(PC)	–
ΔT_r	–	–	–	–	–	–
T_{ti}	+	+	–	–	+	+
P_{ti}	+	+	–	+(RC) +(PC) –(SR)	+	+

sCO_2 inlet temperature of the IHX exceeds 368°C under these conditions, which is unreasonable when the core inlet temperature is 373°C and the IHX pinch temperature difference (ΔT_{IHX}) is 5°C. The performance of different cycles follows similar rules as the design parameters change. As summarized in Table 3, increasing T_{ti} and P_{ti} while decreasing T_{min} and ΔT_r can enhance η_{th}, η_{ex} and W_{net}. The main reason is that raising T_{ti} and P_{ti} raises the cycle average endothermic temperature and the turbine specific work. In addition, the lower the T_{min}, the lower the compressor power consumption, and the lower the ΔT_r, and the better the heat recovery efficiency. On the other hand, it is beneficial to increase ΔT_r to lower V_{HX}. In addition to reducing η_{th}, increasing T_{min} increases m_{sCO_2} and CEP. Therefore, it is best to reduce the T_{min} as much as possible. Although increasing T_{ti} lowers the m_{sCO_2} and the CEP, it also increases V_{HX}. As P_{ti} rises, V_{HX} rises as well. However, the influence of T_{min} on V_{HX} and the effect of P_{ti} on CEP differed between cycles. In contrast to the other two cycles, the PC's V_{HX} reduces as T_{min} increases, while the SR's CEP falls as P_{ti} increases.

If the three cycles are compared, it can be found that RC has the highest η_{th}, η_{ex} and W_{net} under the same design conditions. The PC's η_{th} is 1%–2% lower than the RC's. The SR has the lowest η_{th}, 7%–8% lower than the RC's. Comparing the irreversibility of each cycle component reveals why the RC has high efficiency. As illustrated in Fig. 6, the RC and PC significantly reduce the irreversibility of the recuperators and coolers compared to the SR. The slightly higher efficiency of the RC than

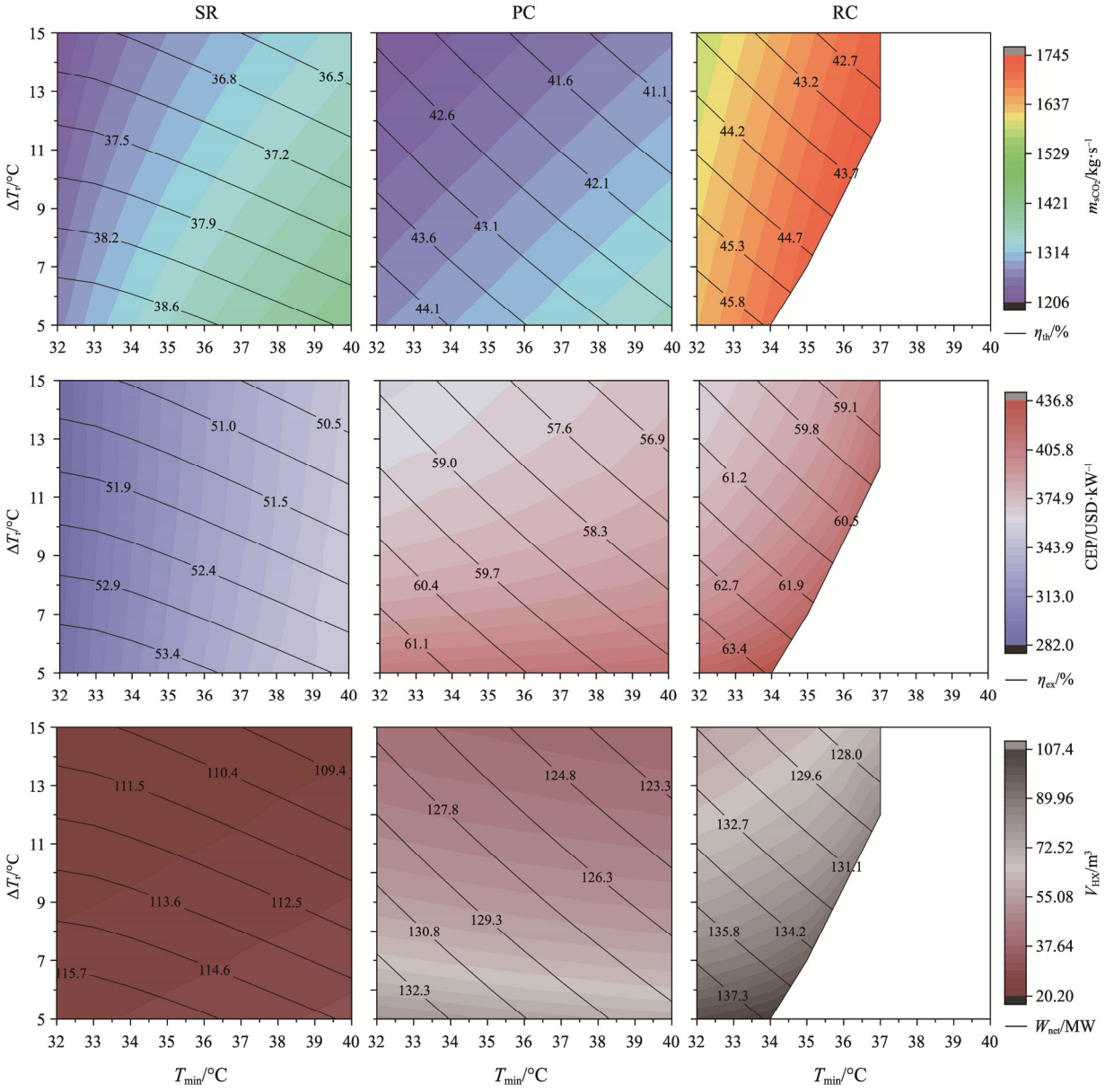

Fig. 4 Performance map of different sCO_2 cycles driven by SFR under different T_{min} and ΔT_r (T_{ti} is 510°C and P_{ti} is 20 MPa)

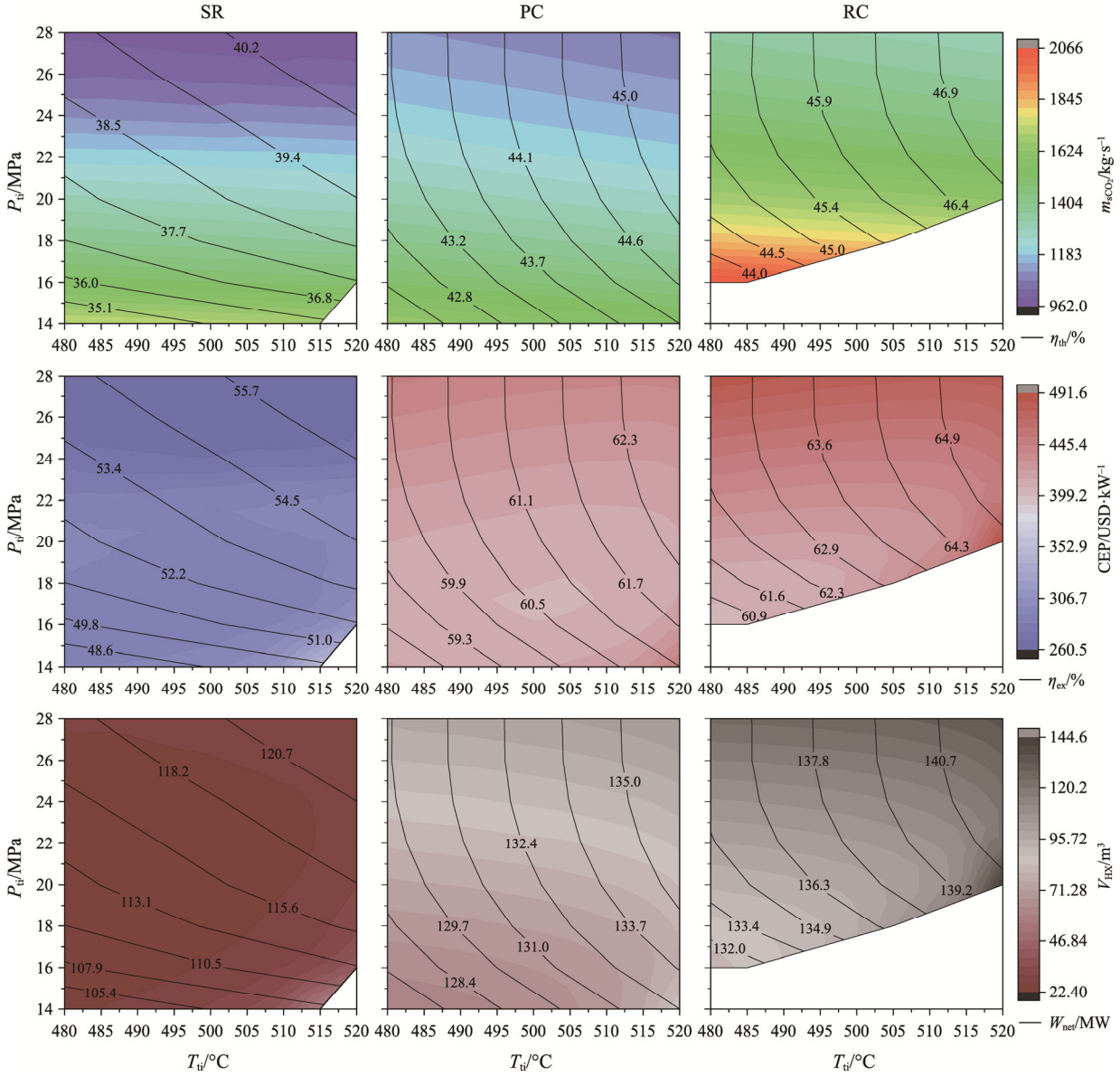

Fig. 5 Performance map of sCO_2 cycles driven by SFR under different T_{ti} and P_{ti} (T_{min} is 32°C and ΔT_r is 5°C)

the PC is mainly due to the lower irreversibility of the reactor in the RC. However, the higher efficiency of the RC comes at the expense of higher m_{sCO_2}, V_{HX} and CEP, as shown in Fig. 4 and Fig. 5. Interestingly, the PC with similar thermal performance to the RC is more advantageous in terms of CEP and V_{HX}, despite the added complexity of an additional compressor. In addition, the SR is undoubtedly the easiest, most economical, and most compact sCO_2 cycle.

4.1.2 Design performance of sCO_2 cycle with PWR

With PWR, changes in design parameters have a similar impact on different sCO_2 cycle performances, as summarized in Table 4. As shown in Fig. 7 and Fig. 8, the W_{net} of sCO_2 cycles coupled with PWR is about 40 MW lower than those with SFR. The ~20% increase in the irreversibility of the PWR reactor in Fig. 6 can well explain the decrease in W_{net} and η_{th} of the sCO_2 cycle coupled to it. In addition, m_{sCO_2} has grown to some extent as the cycle enthalpy rise decreases. Although the V_{HX} of cycles with PWR decreases, CEP increases by 100–140 USD/kW. This means that using SFR improves not only the cycle's efficiency but also its economic performance.

For sCO_2 cycles using PWR, the RC has the highest η_{th}, η_{ex} and W_{net} under the same design conditions. The PC's thermal efficiency is 1%–2% lower than the RC's, and the SR's η_{th} is 3%–6% lower than the RC's. As with SFR, the RC, although the most efficient, also has the highest m_{sCO_2}, V_{HX} and CEP. The SR, while the least efficient, also has the lowest m_{sCO_2}, V_{HX}, and CEP. The PC has similar efficiency to the RC, and its m_{sCO_2}, V_{HX}, and CEP also have advantages over the RC.

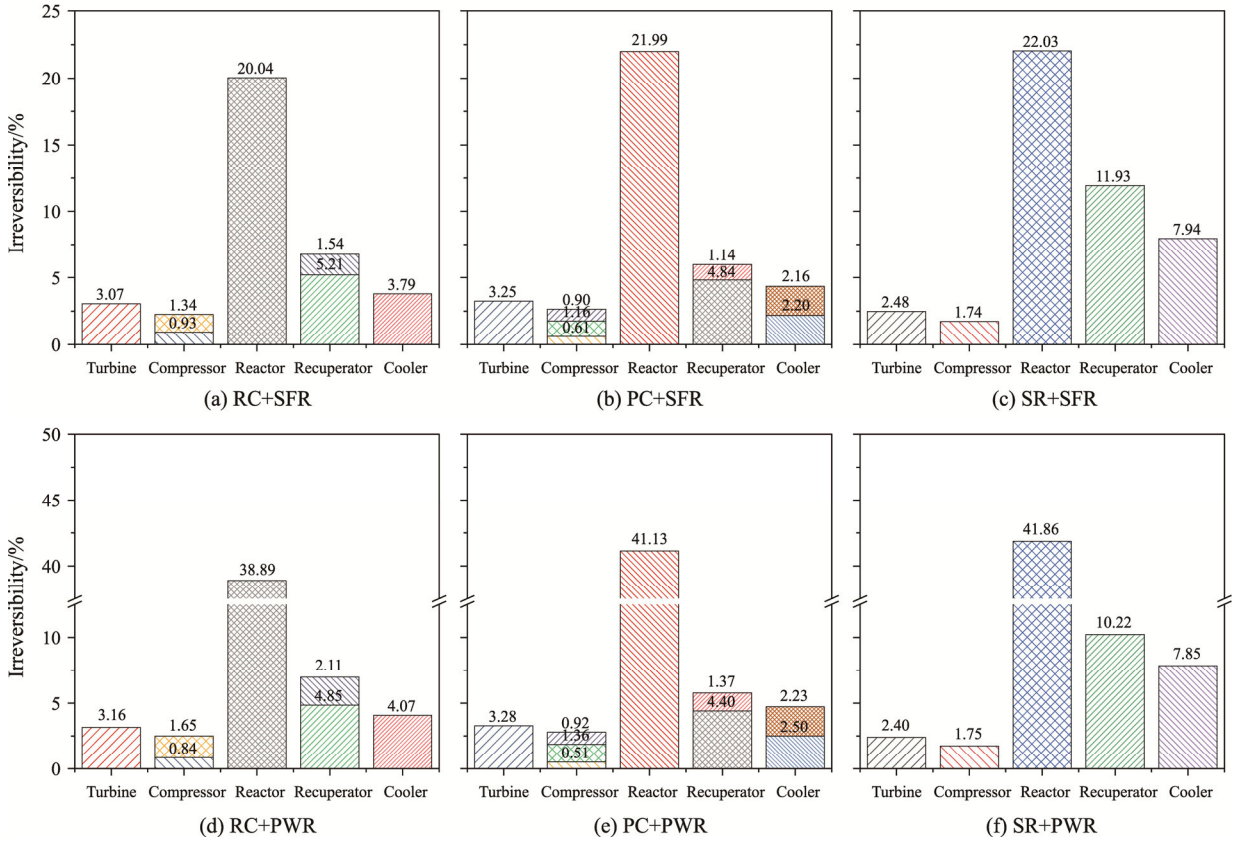

Fig. 6 The irreversibility of sCO_2 cycle components with SFR ($T_{ti}/P_{ti}/T_{min}/\Delta T_r$ is 510°C/20 MPa/32°C/5°C) and PWR ($T_{ti}/P_{ti}/T_{min}/\Delta T_r$ is 310°C/15 MPa/32°C/5°C)

Table 4 Effects of design parameter changes on sCO_2 cycle performance when coupled with PWR

Variables	η_{th}	η_{ex}	m_{sCO_2}	CEP	V_{HX}	W_{net}
T_{min}	–	–	+	+	–(RC) –(PC) +(SR)	–
ΔT_r	–	–	–	–	–	–
T_{ti}	+	+	–	–	+	+
P_{ti}	+	+	–	+	+	+

4.2 Off-design performance

4.2.1 Load-following strategy

The off-design performance analysis of the sCO_2 cycles with SFR is under the condition of 510°C/20 MPa/32°C/5°C for $T_{ti}/P_{ti}/T_{min}/\Delta T_r$, and that with PWR is under the condition of 310°C/15 MPa/32°C/5°C. The design performance is shown in Table 5 and the detailed state parameters of different systems are summarized in Appendix B. The preliminary design of the heat exchangers and compressors under these conditions can be found in Table 6 and Table 7.

For systems using electric propulsion, the turbine's speed remains constant as the load changes to ensure a constant generator frequency. Part-load operation is achieved mainly by changing the turbine flow. Two part-load operation strategies are discussed for the electric propulsion system. The first is a compressor speed and compressor inlet pressure control strategy (Strategy 1) that regulates the turbine mass flow by adjusting the compressor inlet pressure (i.e. turbine outlet pressure) through inventory control and compressor speed control. The other is a turbine bypass control strategy (Strategy 2) that introduces a turbine bypass at HTR cold out (in PC and RC) or recuperator cold outlet (in SR) to reduce the turbine fluid flow and a throttle valve at the turbine outlet to regulate outlet pressure (as the throttle valve and turbine bypass shown in Fig. 1(a), Fig. 1(c), Fig. 1(e)). For systems using mechanical propulsion, different load requirements can be met by changing the rotational speed of the main turbine, and supplemented by the change of the turbine flow to maintain turbine inlet and outlet pressure. When the speed of the main turbine decreases, the total turbine flow can be changed by adjusting the compressor speed (Strategy 3) or by adding a turbine bypass (Strategy 4, as the turbine bypass shown in Fig. 1(b), Fig. 1(d), Fig. 1(f)) to keep the turbine inlet and outlet pressure as the design pressure.

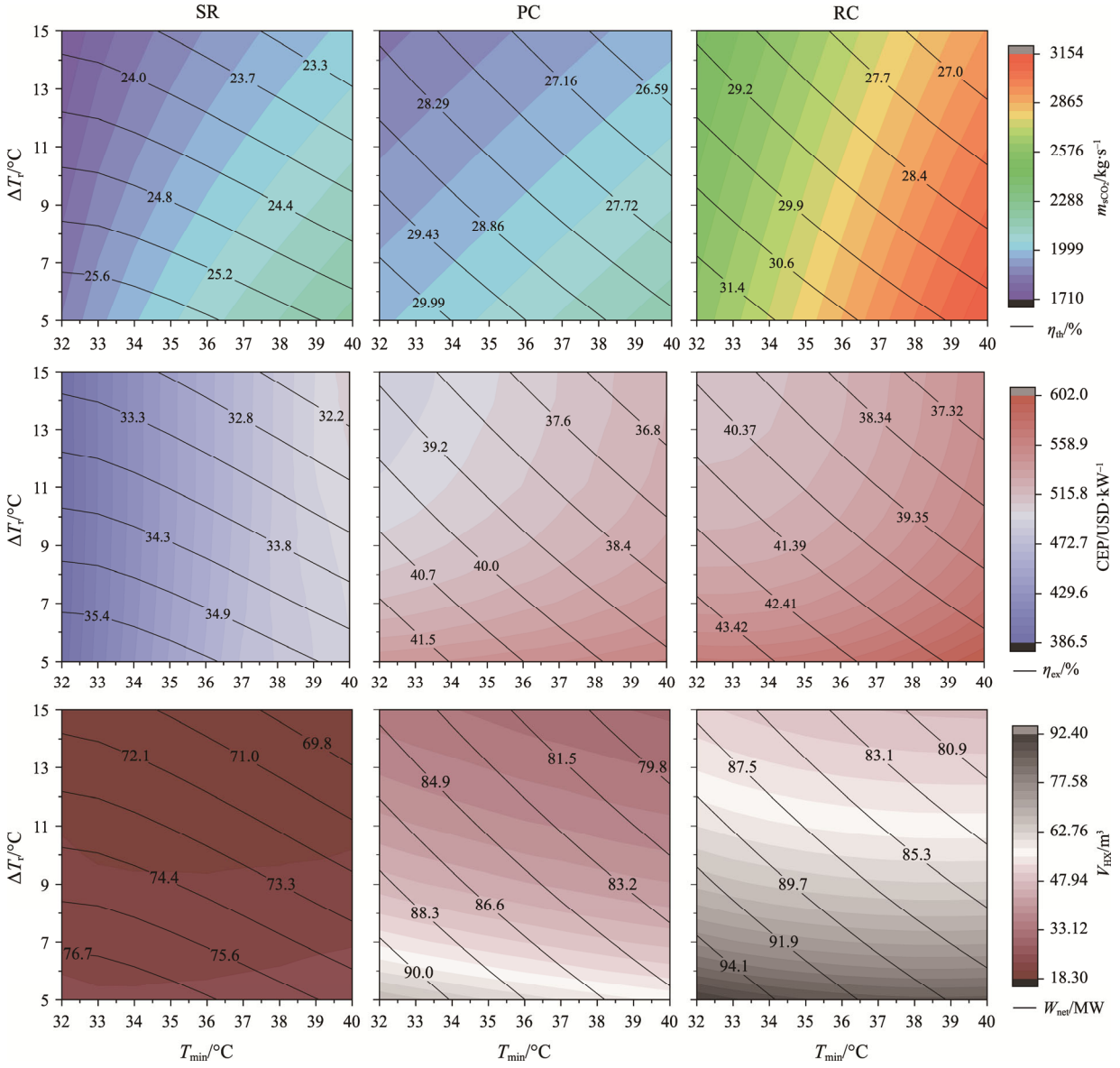

Fig. 7 Performance map of different sCO_2 cycles driven by PWR under different T_{min} and ΔT_r (T_{ti} is 310°C and P_{ti} is 15 MPa)

In addition to the above control strategies, additional controls are required to ensure stable load changes. The core inlet and outlet temperature, i.e. the IHX inlet and outlet temperature of the primary coolant remain constant as the load varies. This is achieved by controlling the primary coolant flow rate and control rod system to avoid large thermal stress on the reactor pressure vessel [16]. The compressor inlet temperature control is realized by coupling the cooler bypass and seawater mass flow rate control [23].

The load ratio is defined as the ratio of the shaft power driving the propeller to the shaft power available to drive the propeller at the design full load condition. Different part-load operation strategies are discussed for different propulsion mode systems as the load ratio varies between 10%–100%. The T_{ti} remains constant as the load varies to avoid large thermal stress on IHX, and P_{ti} also does not vary with load to avoid frequent pressure changes causing fatigue damage to IHX and pipe metal.

4.2.2 Electric propulsion

This work focuses on steady-state performance under off-design conditions. Fig. 9 summarizes the performance and internal parameter changes of the system using the electric propulsion mode when the load changes. As the turbine flow (m_t) decreases (as shown in Fig. 9(g) and Fig. 9(h)), the turbine load and net output power of the system (W_{net}) decrease (as shown in Fig. 9(e) and Fig. 9(f)). At the same time, the turbine outlet pressure (P_{to}) increases (as shown in Fig. 9(i) and Fig. 9(j)). The cycle efficiency (as shown in Fig. 9(a) and

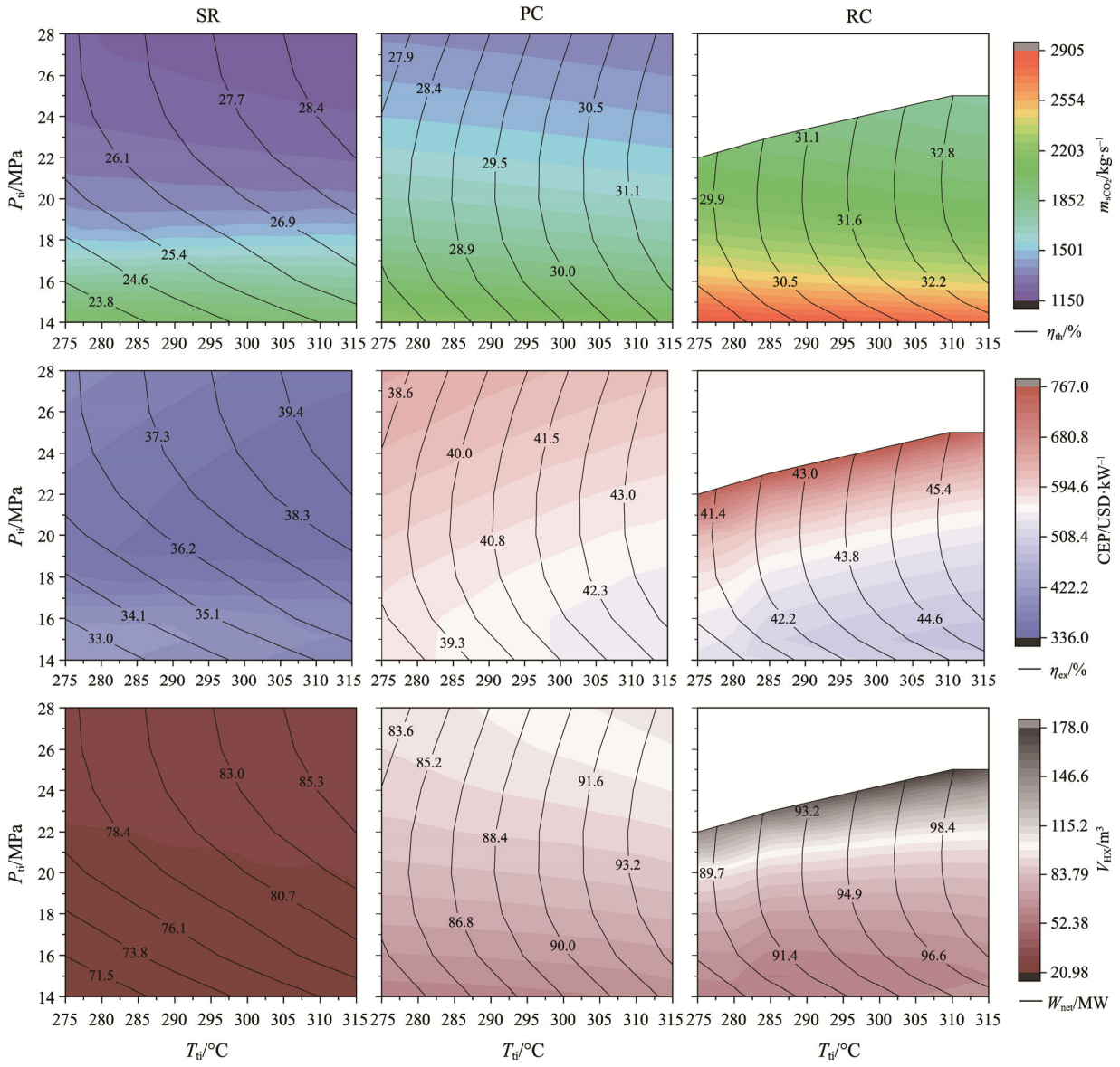

Fig. 8 Performance map of sCO_2 cycles driven by PWR under different T_{ti} and P_{ti} (T_{min} is 32°C and ΔT_r is 5°C)

Table 5 Performance of sCO_2 cycle with SFR ($T_{ti}/P_{ti}/T_{min}/\Delta T_r$ is 510°C/20 MPa/32°C/5°C) and PWR ($T_{ti}/P_{ti}/T_{min}/\Delta T_r$ is 310°C/15 MPa/32°C/5°C)

System	η_{th}/%	η_{ex}/%	m_{sCO2}/kg·s^{-1}	CEP/USD·kW^{-1}	V_{HX}/m^3	W_{net}/MW
SR+SFR	38.91	53.87	1271.93	287.10	25.21	116.72
RC+SFR	46.27	64.07	1635.51	422.70	101.87	138.81
PC+SFR	44.61	61.77	1275.95	409.61	79.22	133.82
SR+PWR	25.94	35.91	1857.75	389.45	23.87	77.81
RC+PWR	32.09	44.43	2593.26	567.95	92.22	96.26
PC+PWR	30.55	42.31	1990.26	542.29	67.26	91.66

Fig. 9(b)) and reactor thermal power (as shown in Fig. 9(c) and Fig. 9(d)) also decrease with decreasing load.

According to Fig. 9, the cycles using Strategy 1 have higher η_{th} compared to the cycles using Strategy 2, but the adjustable load range is limited due to the compressor's surge line. Since the compressor inlet pressure (7.4 MPa) approaches the critical pressure, small changes in inlet pressure and mass flow rate can

Table 6 Detailed compressor design parameters

System	Components	Diameter/mm	Speed/r·min^{-1}	Flow rate/kg·s^{-1}	Enthalpy rise/kJ·kg^{-1}	Power/MW
SR+SFR	MCOM	742	6508	1271.9	33.1	42.1
RC+SFR	MCOM	539	7200	976.4	21.33	20.83
RC+SFR	RCOM	889	7155	659.11	57.41	37.84
PC+SFR	MCOM	432	8697	659.67	20.07	13.24
PC+SFR	RCOM	788	7638	616.28	51.48	31.73
PC+SFR	PCOM	1330	2475	1275.95	15.37	19.61
SR+PMR	MCOM	996	3925	1857.7	21.7	40.31
RC+PMR	MCOM	719	4225	1374.4	13.1	18
RC+PMR	RCOM	1221	4057	1218.8	34.9	42.54
PC+PMR	MCOM	570	5177	891.64	12.35	11.01
PC+PMR	RCOM	1064	4384	1019	30.85	31.44
PC+PMR	PCOM	1695	1559	1990.26	9.9	19.7

Table 7 PCHE details

System	Components	Heat duty/MW	Number of modules	Length of each module/m
SR+SFR	Recuperator	430.00	39	0.92
SR+SFR	Cooler	183.28	24	0.75
SR+SFR	IHX	300	25	0.64
RC+SFR	LTR	196.41	65	2.25
RC+SFR	HTR	437.29	64	1.34
RC+SFR	Cooler	161.19	15	0.65
RC+SFR	IHX	300	41	1.01
PC+SFR	LTR	124.42	61	2.33
PC+SFR	HTR	304.91	50	1.04
PC+SFR	Cooler1	62.50	20	0.32
PC+SFR	Cooler2	103.68	8	0.44
PC+SFR	IHX	300	25	0.65
SR+PMR	Recuperator	348.79	43	0.66
SR+PMR	Cooler	222.19	34	0.78
SR+PMR	IHX	300	28	0.41
RC+PMR	LTR	233.63	85	1.63
RC+PMR	HTR	361.29	73	0.91
RC+PMR	Cooler	203.74	28	1.28
RC+PMR	IHX	300	39	0.39
PC+PMR	LTR	139.99	73	1.65
PC+PMR	HTR	249.68	55	0.70
PC+PMR	Cooler1	84.86	30	0.38
PC+PMR	Cooler2	123.48	11	0.50
PC+PMR	IHX	300	30	0.40

cause compressor surge, making it difficult to achieve variable load operation of SR with Strategy 1. This is why the part-load performance of SR using Strategy 1 is not shown in Fig. 9. In contrast, the system with Strategy 2 can meet the 10%–100% load change requirements because the compressor always works in the design condition as the load varies. However, η_{th} is lower, especially under low load conditions. Taking the RC as an example, the irreversibility shown in Fig. 10 explains the reason for the lower η_{th} when using Strategy 2. It can

be seen that the irreversibility caused by the throttling and mixing process increases rapidly as the load decreases, reaching 32% at the 10% load ratio and becoming the part with the largest exergy loss.

Except for the efficiency differences, m_t is lower and P_{to} is higher in the system using Strategy 1 compared to using Strategy 2. The main reason for this is that the power consumption of the compressors in cycles using Strategy 1 decreases with the decrease of the load because of the reduction in m_{sCO_2}, while it is constant in cycles using Strategy 2. Therefore, for the same W_{net}, the turbine power and m_t of the cycles using Strategy 2 need to be higher than those using strategy 1. In addition, the Q_{th} of cycles using Strategy 1 decreases more than that of cycles using Strategy 2 as the load decreases due to the larger reduction of m_t. Under the same load ratio, the Q_{th} of SFR is lower than that of the PWR.

4.2.3 Mechanical propulsion

Fig. 11 summarizes the performance and internal parameter changes of the system using mechanical propulsion mode as the load changes. The load is reduced by reducing the rotational speed of the MT, while the rotational speed of the AT remains unchanged to maintain

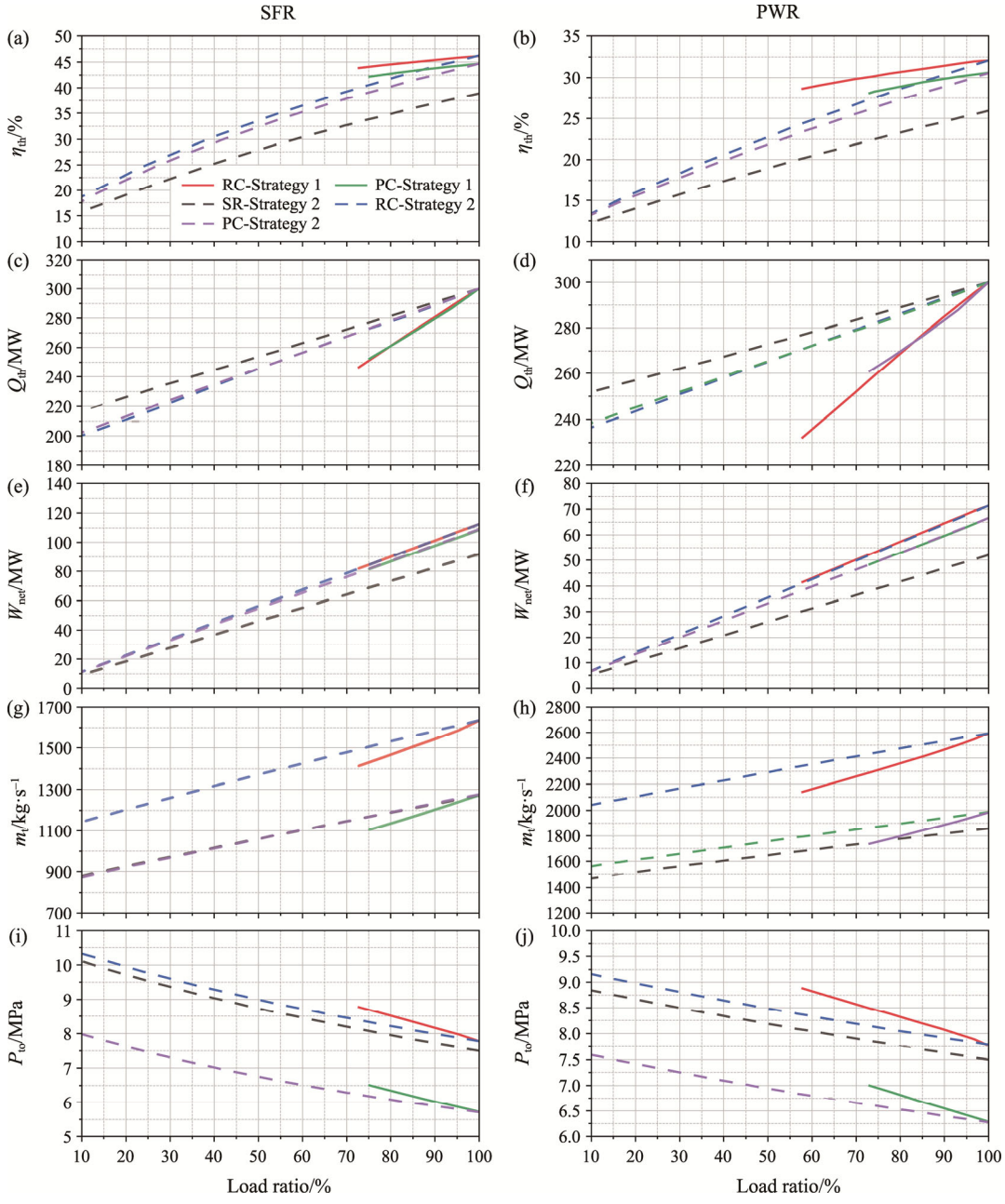

Fig. 9 Part-load performance of sCO_2 cycles with electric propulsion

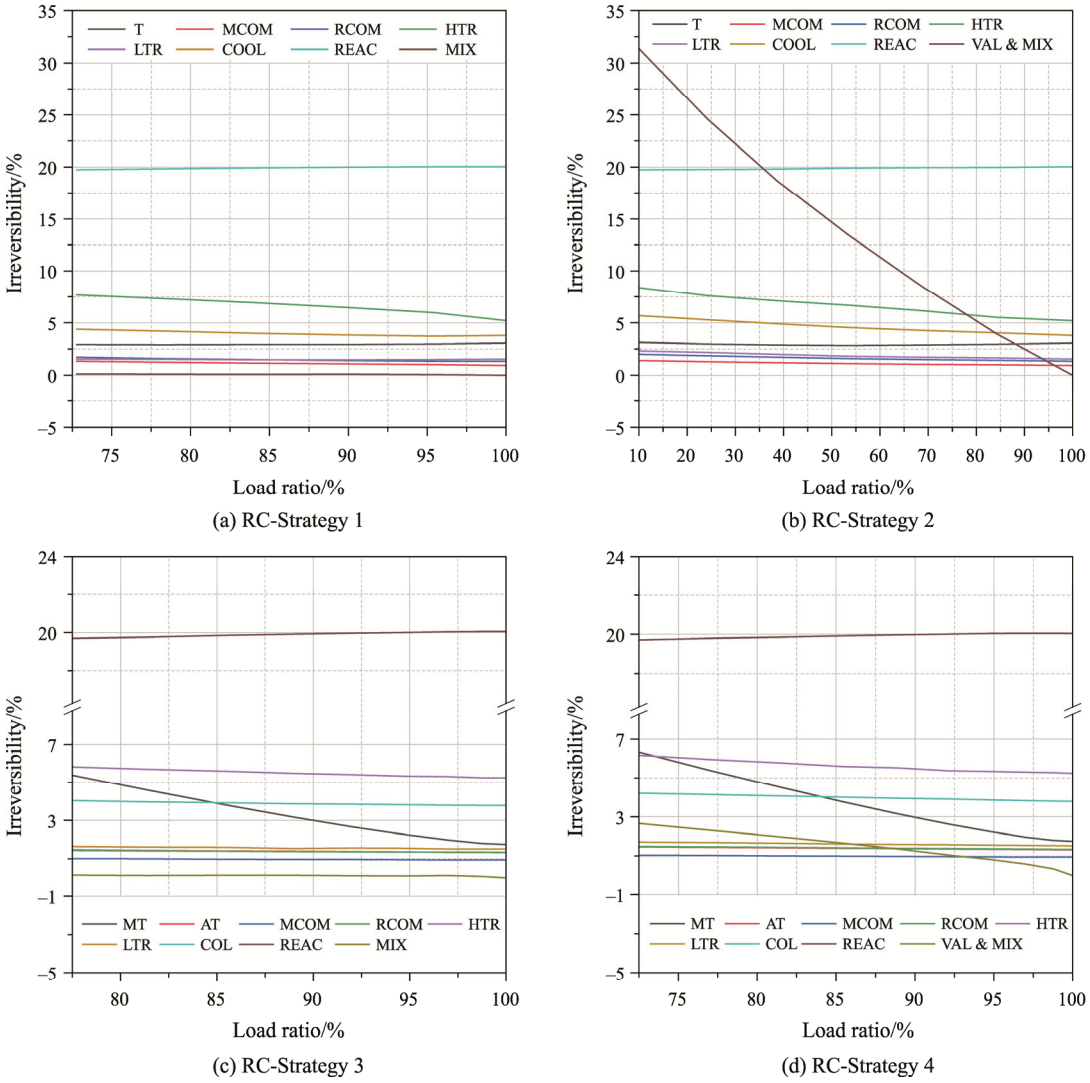

Fig. 10 Irreversibility of cycle components at part-load conditions (MIX means the irreversibility caused by fluid mixing and VAL stands for the irreversibility of throttle and bypass valves)

stable electric power generation. In addition, the power and flow of the auxiliary turbine remain unchanged to meet the needs of power consumption of the compressors, auxiliary machines, and daily electricity consumption. As the W_{MT} decreases for systems using Strategy 3 and Strategy 4, η_{th}, Q_{th} and m_t all decrease, as shown in Fig. 11. The system using Strategy 3 achieves 2%–4% higher η_{th} than that using Strategy 4. The difference in thermal efficiency induced by the two control strategies is mainly caused by the increase in turbine bypass throttling exergy loss when the load drops, as seen in the exergy analysis data in Fig. 10.

Compared with the electric propulsion system, the largest difference in part-load performance is that the PC and the SR with the mechanical propulsion mode could achieve load changes in the range of 10%–100% no matter which control strategy is used. This is because the compressor flow change is smaller in the mechanical propulsion mode than in the electric propulsion mode. When the load ratio changes between 100% and 10%, the compressor flow rate is always greater than the surge flow limit. However, the load ratio of the RC with SFR can only drop to 77% and 72% using Strategy 3 and Strategy 4, because the IHX inlet sCO_2 temperature rises as the load decreases, gradually exceeding the maximum allowable temperature (Core inlet temperature+ΔT_{IHX}). Interestingly, under the same load ratio, the η_{th} of the system using Strategy 2 and the system using Strategy 4 is very close. Although the throttling exergy loss of the mechanical propulsion mode is not as large as that of the electric propulsion mode, the exergy loss in the turbine is higher in the mechanical propulsion mode, as demonstrated in Fig. 10. The trade-off results in basically the same efficiency.

4.3 Discussion on the configuration of nuclear-powered sCO_2 cycle marine propulsion system

Previous studies on the use of the sCO_2 cycle in nuclear power plants have generally favoured the recompression cycle due to its higher efficiency. However, evaluation from various dimensions such as volume, weight, CEP, and part-load performance suggests that the PC and SR cycles may be more suitable for use in nuclear-powered ships. While the RC cycle has the highest output work and thermal efficiency at full and part load, it is not as advantageous in terms of volume, weight, and cost, and there are also more restrictions on

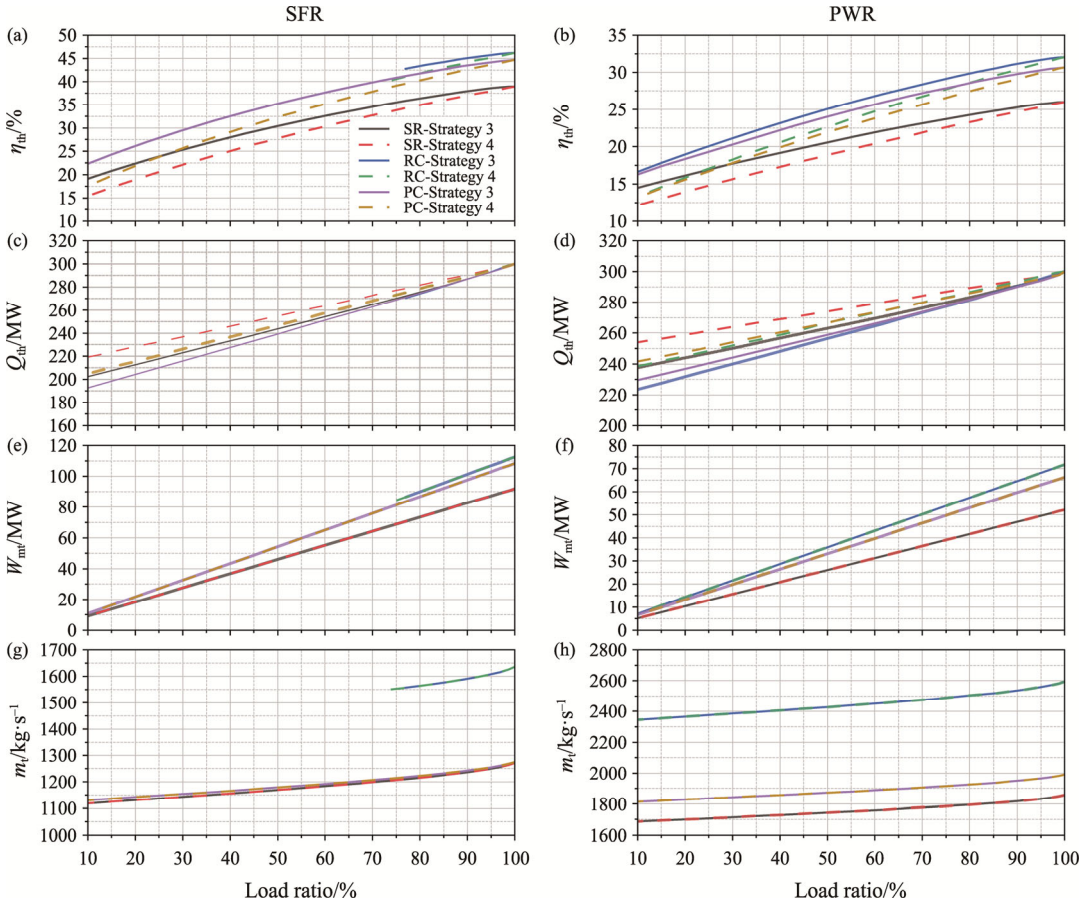

Fig. 11 Part-load performance of sCO_2 cycles with mechanical propulsion

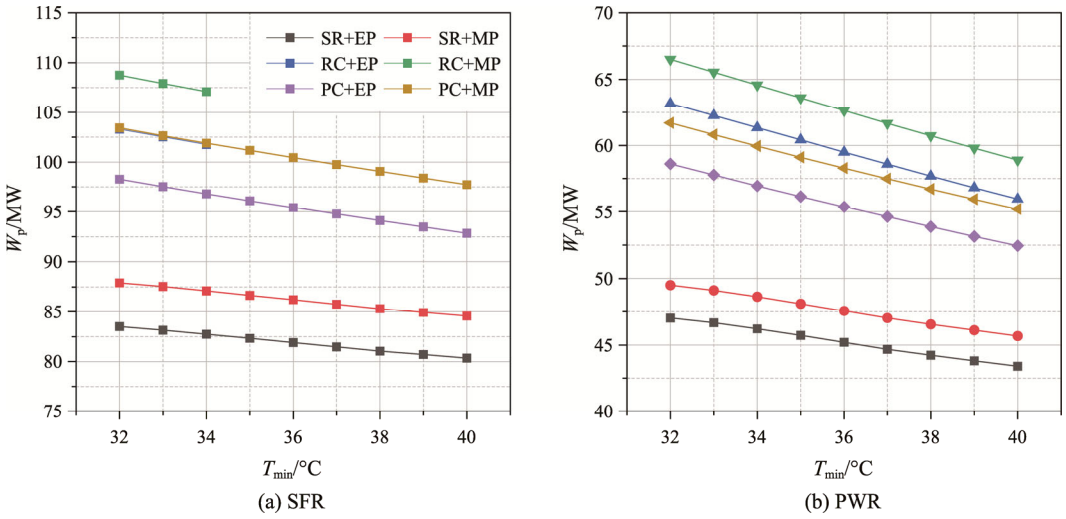

Fig. 12 Propeller shaft power for electrical propulsion mode and mechanical propulsion mode

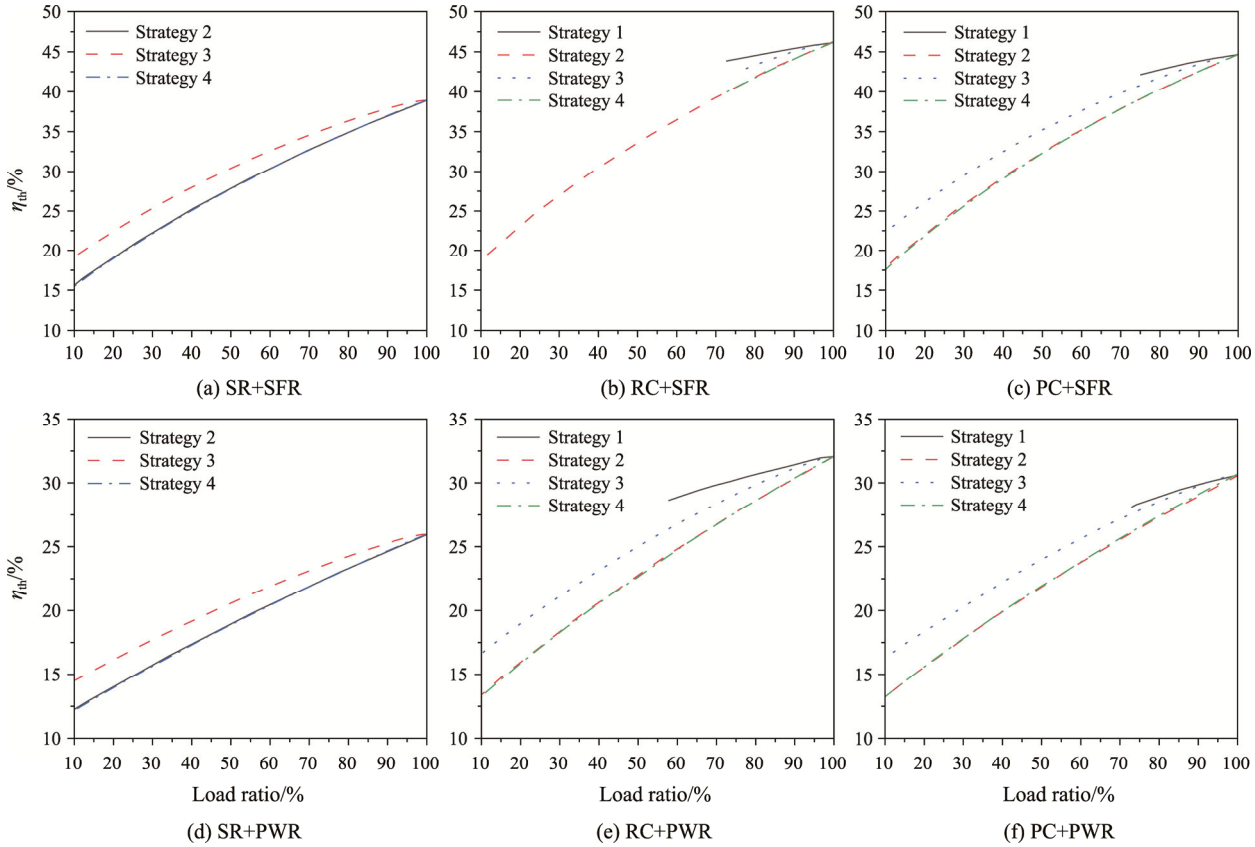

Fig. 13 Comparison of thermal efficiency when different load-following strategies used

its design parameters and load adjustment. The PC cycle is slightly less efficient than the RC cycle (by about 1%–2%), but it offers advantages in terms of volume, weight, cost, and flexibility of load adjustment. The SR cycle has the lowest thermal efficiency at design and part-load conditions (about 6%–8% lower than the RC cycle under the same conditions), but it is significantly more compact, with a V_{HX} that is reduced by 70%–75% compared to the RC cycle and a CEP that is reduced by about 30%.

In terms of propulsion mode and load control strategy, electric propulsion systems tend to have larger power losses in the transmission between the turbine and the propeller compared to mechanical propulsion systems. For instance, Fig. 12 shows that the propeller shaft power in the electric propulsion mode is 2.4 MW–5.5 MW lower than in the mechanical propulsion mode as T_{min} varies. For electric propulsion systems, bypass control has to be used to enable 10%–100% load changes. In mechanical propulsion systems, the load can be adjusted by adjusting the main turbine speed, with bypass control and compressor speed control serving as auxiliary means to stabilize inlet and outlet turbine pressure. Fig. 13 shows the thermal efficiency of different sCO_2 cycles in nuclear-powered ships under various load-following strategies. It can be seen that Strategy 1 yields the highest η_{th}, followed by Strategy 3, with the lowest η_{th} resulting from Strategies 2 and 4. Overall, Strategy 3 offers the most flexibility and efficiency among the four strategies.

5. Conclusions

Unlike applications in nuclear power plants, the sCO_2 cycle for nuclear-powered ships needs to be more compact and flexible. This paper presents a study on the design and selection of suitable sCO_2 cycles for nuclear-powered ships. Taking into account the characteristics of nuclear-powered ships, the paper evaluates the thermodynamic performance, cost, volume, weight, and part-load performance of several nuclear-powered sCO_2 cycles using various indicators, and compares four different load-following strategies. The main findings are as follows:

(1) The recompression cycle (RC) and the partial cooling cycle (PC) have similar thermal efficiency (η_{th}), but the PC has advantages in terms of heat exchanger volume (V_{HX}) and the capital cost of every unit of cycle output power (CEP). Although the η_{th} of the simple recuperated cycle (SR) differs from that of the RC and PC by 6%–8%, it has a simpler structure and lower V_{HX}

and CEP. The system using a sodium-cooled fast reactor (SFR) has not only higher efficiency but also lower CEP than the system using a pressurized water reactor (PWR).

(2) When Strategy 1 or Strategy 2 is used, the configuration of the sCO_2 cycle applied to nuclear-powered ships is similar to that used in nuclear power plants, because the turbine output work is all converted into electrical energy. Strategy 2 can achieve a load ratio change from 100%–10%, but Strategy 1 cannot reduce the load ratio below 70% due to the limitation of the compressor surge line.

(3) Adopting Strategy 3 and Strategy 4 can effectively avoid the compressor state point close to the surge point, enabling the system to operate at load ratios from 100% to 10%. Among the four control strategies, Strategy 3 makes the cycle more efficient and flexible.

(4) The PC is more suitable for nuclear-powered ships because it offers high thermal efficiency and low volume and cost, and maintains relatively high thermal efficiency at part load.

This study focuses on the steady-state characteristics of the nuclear-powered sCO_2 marine propulsion system, but it is also essential to consider the system's dynamic response to changes in load demand. Future research should aim to investigate the dynamic behaviour of this system and its potential applications in nuclear-powered ships.

Acknowledgements

This work was supported by the National Natural Science Foundation of China (52276150).

Conflict of Interest

On behalf of all authors, the corresponding author states that there is no conflict of interest.

Electronic Supplementary Materials

Supplementary materials are available in the online version of this article at

https://doi.org/10.1007/s11630-023-1896-6

References

[1] IMO. Fourth IMO Greenhouse Gas Study. International maritime organization, London, 2021.

[2] Yoon H.J., Ahn Y., Lee J.I., Addad Y., Potential advantages of coupling supercritical CO_2 Brayton cycle to water cooled small and medium size reactor. Nuclear Engineering and Design, 2012, 245: 223–232.

[3] Oh B.S., Kim Y., Kim S.J., Lee J.I., SMART with trans-critical CO_2 power conversion system for maritime propulsion in Northern Sea Route, part 1: System design. Annals of Nuclear Energy, 2020, 149(15): 107792.

[4] Du Y., Yang C., Hu C., Zhang C., Thermoeconomic analysis and inter‐stage pressure ratio optimization of nuclear power supercritical CO_2 multi‐stage recompression. International Journal of Energy Research, 2020, 45(2): 2367–2382.

[5] Du Y., Yang C., Hu C., Zhou M., Thermodynamic design and Off-design investigation of nuclear power supercritical CO_2 recompression cycle. Nuclear Engineering and Design, 2020, 369(1): 110851.

[6] Park J.H., Park H.S., Kwon J.G., et al., Optimization and thermodynamic analysis of supercritical CO_2 Brayton recompression cycle for various small modular reactors. Energy, 2018, 160: 520–535.

[7] Floyd J., Alpy N., Moisseytsev A., et al., A numerical investigation of the sCO_2 recompression cycle off-design behaviour, coupled to a sodium cooled fast reactor, for seasonal variation in the heat sink temperature. Nuclear Engineering and Design, 2013, 260: 78–92.

[8] Guo Z., Zhao Y., Zhu Y., et al., Optimal design of supercritical CO_2 power cycle for next generation nuclear power conversion systems. Progress in Nuclear Energy, 2018, 108: 111–121.

[9] Lee J., Lee J.I., Yoon H.J., et al., Supercritical carbon dioxide turbomachinery design for water-cooled small modular reactor application. Nuclear Engineering and Design, 2014, 270: 76–89.

[10] Li M., Jie Y., Zhu H., et al., The thermodynamic and cost-benefit-analysis of miniaturized lead-cooled fast reactor with supercritical CO_2 power cycle in the commercial market. Progress in Nuclear Energy, 2018, 103: 135–150.

[11] Li M., Xu J., Cao F., et al. The investigation of thermo-economic performance and conceptual design for the miniaturized lead-cooled fast reactor composing supercritical CO_2 power cycle. Energy, 2019, 173: 174–195.

[12] Luo D., Huang D., Thermodynamic and exergoeconomic investigation of various SCO_2 Brayton cycles for next generation nuclear reactors. Energy Conversion and Management, 2020, 209(1): 112649.

[13] Dostal V., Driscoll M.J., Hejzlar P., A supercritical carbon dioxide cycle for next generation nuclear reactors. Massachusetts Institute of Technology, Boston, USA, 2004.

[14] Moisseytsev A., Sienicki J.J., Transient accident analysis of a supercritical carbon dioxide Brayton cycle energy converter coupled to an autonomous lead-cooled fast reactor. Nuclear Engineering and Design, 2008, 238(8): 2094–2105.

[15] Moisseytsev A., Sienicki J.J., Investigation of alternative

layouts for the supercritical carbon dioxide Brayton cycle for a sodium-cooled fast reactor. Nuclear Engineering and Design, 2009, 239(7): 1362–1371.

[16] Wu P., Ma Y., Gao C., et al., A review of research and development of supercritical carbon dioxide Brayton cycle technology in nuclear engineering applications. Nuclear Engineering and Design, 2020, 368: 110767.

[17] Li Z., Liu X., Shao Y., Zhong W., Research and development of supercritical carbon dioxide coal-fired power systems. Journal of Thermal Science, 2020, 29(3): 546–575.

[18] Combs O.V., An investigation of the supercritical CO_2 cycle (Feher cycle) for shipboard application. Massachusetts Institute of Technology, Boston, USA, 1977.

[19] Oh B.S., Kim S.J., Kim Y., Lee J.I., SMART with trans-critical CO_2 power conversion system for maritime propulsion in Northern Sea Route, part 2: Transient analysis. Annals of Nuclear Energy, 2021, 150: 107875.

[20] Pérez-Pichel G.D., Linares J.I., Herranz L.E., Moratilla B.Y., Thermal analysis of supercritical CO_2 power cycles: Assessment of their suitability to the forthcoming sodium fast reactors. Nuclear Engineering and Design, 2012, 250: 23–34.

[21] Zhu H., Xie G., Yuan H., Nizetic S., Thermodynamic assessment of combined supercritical CO_2 cycle power systems with organic Rankine cycle or Kalina cycle. Sustainable Energy Technologies and Assessments, 2022, 52: 102166.

[22] Pham H.S., Alpy N., Ferrasse J.H., et al., Mapping of the thermodynamic performance of the supercritical CO_2 cycle and optimisation for a small modular reactor and a sodium-cooled fast reactor. Energy, 2015, 87: 412–424.

[23] Moisseytsev A., Sienicki J.J., Dynamic control analysis of the AFR-100 SMR SFR with a supercritical CO_2 cycle and dry air cooling: part I — plant control optimization. 26th International Conference on Nuclear Engineering, London, UK, 2018.

[24] Oh B.S., Ahn Y.H., Yu H., et al., Safety evaluation of supercritical CO_2 cooled micro modular reactor. Annals of Nuclear Energy, 2017, 110: 1202–1216.

[25] Baek J.Y., Lee J.J., Lee J.I., Transient analyses of the S-CO_2 Cycle coupled to PWR for nuclear marine propulsion. Transactions of the Korean Nuclear Society Virtual Spring Meeting, Republic of Korea, 2020.

[26] Carstens N., Control strategies for supercritical carbon dioxide power conversion systems. Massachusetts Institute of Technology, Boston, USA, 2007.

[27] Lock A., Bone V., Off-design operation of the dry-cooled supercritical CO_2 power cycle. Energy Conversion and Management, 2022, 251: 114903.

[28] Thanganadar D., Fornarelli F., Camporeale S., et al., Off-design and annual performance analysis of supercritical carbon dioxide cycle with thermal storage for CSP application. Applied Energy, 2021, 282: 116200.

[29] Wan X., Wang K., Zhang C.M., et al., Off-design optimization for solar power plant coupling with a recompression supercritical CO_2 Brayton cycle and a turbine-driven main compressor. Applied Thermal Engineering, 2022, 209: 118281.

[30] Yang J., Yang Z., Duan Y., Off-design performance of a supercritical CO_2 Brayton cycle integrated with a solar power tower system. Energy, 2020, 201: 117676.

[31] Yang J., Yang Z., Duan Y., Part-load performance analysis and comparison of supercritical CO_2 Brayton cycles. Energy Conversion and Management, 2020, 214: 112832.

[32] Yu J.C., Marine nuclear power technology. Shanghai Jiaotong University Press, Shanghai, 2016.

[33] Aoto K., Uto N., Sakamoto Y., et al., Design study and R&D progress on Japan sodium-cooled fast reactor. Journal of Nuclear Science and Technology, 2011, 48(4): 463–471.

[34] White M.T., Bianchi G., Chai L., et al., Review of supercritical CO_2 technologies and systems for power generation. Applied Thermal Engineering, 2021, 185: 116447.

[35] Ragheb M., Nuclear Naval Propulsion. IntechOpen, London, 2011.

[36] Nuclear-Powered Ships. https://world-nuclear.org/information-library/non-power-nuclear-applications/transport/nuclear-powered-ships.aspx, 2021 (accessed on March 13, 2023).

[37] Grandy C., Kim T.K., Jin E., et al., Advanced fast reactor - 100 - design overview. International Atomic Energy Agency (IAEA), New York, 2015.

[38] Molland A.F., Marine engines and auxiliary machinery. The Maritime Engineering Reference Book, Oxford, Butterworth-Heinemann, 2008, pp. 344–482.

[39] Xu J., Sun E., Li M., et al, Key issues and solution strategies for supercritical carbon dioxide coal fired power plant. Energy, 2018, 157: 227–246.

[40] Demirel Y., Energy: production, conversion, storage, conservation, and coupling. Springer Science & Business Media, 2012.

[41] Roshanfekr P., Lundmark S., Thiringer T., et al., A synchronous reluctance generator for a wind application-compared with an interior mounted permanent magnet synchronous generator. 7th IET International Conference on Power Electronics, Machines and Drives (PEMD 2014), Manchester, UK, 2014, pp. 1–5. DOI: 10.1049/cp.2014.0411.

[42] Pabiszczak S., Kowal M., Efficiency of the eccentric rolling transmission. Mechanism and Machine Theory, 2022, 169: 104655.

[43] Mikityuk K., Heat transfer to liquid metal: Review of data and correlations for tube bundles. Nuclear Engineering and Design, 2009, 239(4): 680–687.

[44] Wang Y., Xie G., Zhu H., et al., Assessment on energy and exergy of combined supercritical CO_2 Brayton cycles with sizing printed-circuit-heat-exchangers. Energy, 2023, 263: 125559.

[45] Wright S.A., Radel R.F., Vernon M.E., et al., Operation and analysis of a supercritical CO_2 Brayton cycle. Sandia report, USA, 2010. DOI:10.2172/984129

[46] Pham H.S., Alpy N., Ferrasse J.H., et al., An approach for establishing the performance maps of the sc-CO_2 compressor: Development and qualification by means of CFD simulations. International Journal of Heat and Fluid Flow, 2016, 61: 379–394.

[47] Dyreby J.J., Modeling the supercritical carbon dioxide Brayton cycle with recompression. The University of Wisconsin-Madison, Madison, USA, 2014.

[48] Fuller R., Preuss J., Noall J., Turbomachinery for supercritical CO_2 power cycles. American Society of Mechanical Engineers, 2012, 44717: 961–966. DOI: 10.1115/GT2012-68735

[49] Arenas Pinilla E.M., Cantizano González A., Asenjo Pedraza I., et al., Design and analysis of radial and axial turbomachinery of supercritical CO_2 power cycles. http://hdl.handle.net/11531/36538, 2019.

[50] Liu J., Yan S., Zeng D., A new measurement model for main steam flow of power plants. Procedia Environmental Sciences, 2011, 11: 18–24.

[51] Li S., Wang Z., Gas turbine performance analysis. Harbin Institute of Technology Press, Harbin, 2017.

[52] Carlson M.D., Middleton B.M., Ho C.K., Techno-economic comparison of solar-driven SCO_2 Brayton cycles using component cost models baselined with vendor data and estimates. ASME 2017 11th International Conference on Energy Sustainability. DOI: 10.1115/ES2017-3590

[53] Sarkar J., Second law analysis of supercritical CO_2 recompression Brayton cycle. Energy, 2009, 34(9): 1172–1178.